

### **Geophysical Research Letters**\*



#### RESEARCH LETTER

10.1029/2024GL110190

#### **Key Points:**

- Quasi-synoptic submesoscaleresolving observations reveal strong upward vertical heat transport (VHT) in the ocean interior (over nearly 10x the mixed layer depth (MLD))
- Submesoscale fronts (<30 km) between eddies act as the primary driver for enhanced vertical heat transport >100 W m<sup>-2</sup>
- There is a significant imbalance in VHT associated with oceanic mesoscale, submesoscale, and mixing processes

#### **Supporting Information:**

Supporting Information may be found in the online version of this article.

#### Correspondence to:

Z. Jing, jingzhiyou@scsio.ac.cn

#### Citation:

Cao, H., Jing, Z., & Fox-Kemper, B. (2024). Scale-dependent vertical heat transport inferred from quasi-synoptic submesoscale-resolving observations. *Geophysical Research Letters*, *51*, e2024GL110190. https://doi.org/10.1029/2024GL110190

Received 7 MAY 2024 Accepted 7 JUN 2024

# © 2024. The Author(s). This is an open access article under the terms of the Creative Commons Attribution-NonCommercial-NoDerivs License, which permits use and distribution in any medium, provided the original work is properly cited, the use is non-commercial and no modifications or adaptations are made.

## Scale-Dependent Vertical Heat Transport Inferred From Quasi-Synoptic Submesoscale-Resolving Observations

Haijin Cao<sup>1,2</sup>, Zhiyou Jing<sup>3</sup>, and Baylor Fox-Kemper<sup>4</sup>

<sup>1</sup>Key Laboratory of Marine Hazards Forecasting, Ministry of Natural Resources, Hohai University, Nanjing, China, <sup>2</sup>College of Oceanography, Hohai University, Nanjing, China, <sup>3</sup>State Key Laboratory of Tropical Oceanography, South China Sea Institute of Oceanology, Chinese Academy of Sciences, Guangzhou, China, <sup>4</sup>Department of Earth, Environmental, and Planetary Sciences, Brown University, Providence, RI, USA

**Abstract** Oceanic motions across meso-, submeso-, and turbulent scales play distinct roles in vertical heat transport (VHT) between the ocean's surface and its interior. While it is commonly understood that during summertime the enhanced stratification due to increased solar radiation typically results in an reduced upper-ocean vertical exchange, our study reveals a significant upward VHT associated with submesoscale fronts (<30 km) through high-resolution observations in the eddy-active South China Sea. The observation-based VHT reaches  $\sim 100 \text{ W m}^{-2}$  and extends to  $\sim 150 \text{ m}$  deep at the fronts between eddies. Combined with microstructure observations, this study demonstrates that mixing process can only partly offset the strong upward VHT by inducing a downward heat flux of  $0.5-10 \text{ W m}^{-2}$ . Thus, the submesoscale-associated VHT is effectively heating the subsurface layer. These findings offer a quantitative perspective on the scale-dependent nature of VHT, with crucial implications for the climate system.

Plain Language Summary Understanding the upper-ocean heat budget is of great importance for gaining insight into how oceanic processes modulate the climate system, yet vertical heat transport (VHT) by submesoscale processes remains rarely studied using observations. Recently, scientists have identified the potential importance of submesoscale instabilities to enhance upward VHT within the mixed layer. However, the vertical pathways of heat from the ocean interior to the surface and the underlying mechanisms remain unclear, largely due to the limitations in observing such small, fast scales. To elucidate these questions, we conducted high-resolution (a horizontal resolution of ~0.6 km), synoptic in-situ observations targeted at submesoscale phenomena near mesoscale eddies. Our study reveals substantial contributions of submesoscale processes to upward VHT in the stratified subsurface layer. This causes a notable imbalance in VHT by mesoscale, submesoscale, and mixing processes. These findings provide valuable insights for enhancing our understanding of heat uptake in the ocean.

#### 1. Introduction

The upper ocean heat budget directly influences the sea surface temperature and air-sea heat exchange, thereby impacting the climate state (Griffies et al., 2015). The rate of ocean heat uptake relies on oceanic motions across a broad range of scales from centimeters to kilometers (Ferrari & Wunsch, 2009; Klein & Lapeyre, 2009). Mesoscale eddies in the ocean play a crucial role in both lateral (poleward) heat transport (e.g., Bryan, 1996; Dong et al., 2014; Jayne & Marotzke, 2002), and vertical heat transport (VHT) (Griffies et al., 2015; Jing et al., 2020; Klein et al., 2008; Li et al., 2021; Qu et al., 2022; Wolfe et al., 2008). These eddy activities are thought to drive a substantial upward VHT to compensate the downward heat transport by large-scale wind-driven vertical circulation and small-scale vertical diffusion (Griffies et al., 2015; Wunsch & Ferrari, 2004).

However, recent studies have suggested that submesoscale processes tend to be more effective in driving VHT, both within and below the mixed layer (Cao & Jing, 2022; Fox-Kemper et al., 2008; Siegelman et al., 2020; Su et al., 2018, 2020; Wang et al., 2022; Yang et al., 2021; Yu et al., 2019), as a consequence of enhanced vertical flows typically ranging from 10 to 100 m day<sup>-1</sup>. During the wintertime, submesoscale motions associated with mixed-layer instabilities (Boccaletti et al., 2007) can drive extremely strong upward VHT (Su et al., 2018, 2020; Yang et al., 2021). These submesoscale processes have been successfully parameterized in ocean models (Bodner et al., 2023; Fox-Kemper et al., 2008, 2011). Yet, note that this mechanism operates primarily within the mixed layer. In the summer when the mixed layer is shallow, submesoscale VHT is typically considered less significant (Bodner et al., 2023; Callies et al., 2015; Dong et al., 2020; Su et al., 2020), but submesoscale fronts remain

19448007, 2024, 12, Downloaded from https://agupubs.onlinelibrary.wiley.com/doi/10.1029/2024GL110190, Wiley Online Library on [17/06/2024]. See the Terms and Conditions

**Figure 1.** (a) Map showing the observation locations and sea level anomaly from AVISO on 19 May 2023. The black solid lines delineate the routes of underwater towed TRIAXUS observations, while the triangles indicate the positions where conductivity temperature depth and vertical microstructure profiler data were collected. (b) Sectional view of temperature acquired through the TRIAXUS across the eddy (S1, S2, and S3) and at the fronts between eddies (F1-F7) over the upper 200 m. The observed temperature sections have a along-track resolution of approximately 0.6 km.

ubiquitous in the ocean interior, particularly in energetic regions such as the Kuroshio Extension, the Gulf Stream, and the Antarctic Circumpolar Current (Ferrari, 2011). In these regions, subsurface frontogenesis associated with the confluence of background flows can lead to the development of ageostrophic secondary circulation in response to front intensification. This circulation pattern induces upwelling on the warmer side of the front and downwelling on the colder side (Cao & Jing, 2022; Klein et al., 2008; Ramachandran et al., 2014), ultimately resulting in a net upward VHT in the oceanic interior. Supporting this notion, Siegelman et al. (2020), using sea seal data, demonstrated that deep-reaching submesocale fronts in the Antarctic Circumpolar Current can trigger a transient upward VHT rate as high as 2000 W m<sup>-2</sup>. However, it is essential to note that this observation is not quasi-synoptic, potentially introducing errors in diagnosing submesocale processes. To date, in terms of limited observational evidence, the relative importance of multi-scale processes in governing the vertical heat exchange between the surface and the ocean interior remains an open question.

Using high-resolution observations targeted at submesoscale processes in the eddy-rich South China Sea during the summer season, this study evaluates the VHT over the upper 200 m, mostly within the thermocline. The results demonstrate that mesoscale and submesoscale processes can efficiently transport heat upward from the ocean interior to the surface, continuously heating the surface in the eddy-rich region. It is found that there is a significant imbalance in subsurface VHT associated with oceanic mesoscale, submesoscale, and mixing processes. The enhanced upward VHT below the mixed layer is predominantly associated with the deep-reaching submesoscale fronts, and we also discuss the underlying dynamics responsible for the VHT.

#### 2. Data and Methods

#### 2.1. Data

From May 8–26, 2023, a field campaign was carried out according to the satellite altimeter data (AVISO, Figure S3 in Supporting Information S1) to capture mesoscale and submesoscale features in the eddy-rich South China Sea. We used an underwater towed vehicle TRIAXUS on board R/V SHIYAN6 (Figure 1a) to collect Conductivity Temperature Depth (CTD) data across an anticyclonic eddy (Figures S1–S3 in Supporting Information S1, from May 11 through May 14) and the fronts between eddies (F1-F7, from May 19 through May 20). The TRIAXUS, performing saw-tooth shaped undulation down to 200 m, measured temperature, conductivity, and pressure, with each cycle lasting approximately 5.5 min while crushing at a speed of  $\sim$ 6.5 knots (2 casts within  $\sim$ 1,100 m). As demonstrated in Figure S4 in Supporting Information S1, the rapid survey within a few days can be regarded as quasi-synoptic, minimizing errors caused by smearing and aliasing effects in low-speed observations such as those by underwater gliders (Rudnick & Cole, 2011). So synopticity throughout the survey is crucial for diagnosing and analyzing submesoscale processes (Cutolo et al., 2022). The fast-sampling data along the ship track

CAO ET AL. 2 of 9

were interpolated onto a grid of 0.6 km in the along-track direction and a vertical grid of 0.2 m, thus resolving most submesoscale features (Figure 1b). Error levels are estimated in the Supporting Information S1.

During the campaign, 23 CTD casts were collected using a Sea-Bird SBE 9 along the crossover lines within the eddy (marked as triangles in Figure 1a). In conjunction with the CTD casts, a free-falling Rockland Scientific vertical microstructure profiler (VMP-250) was used to measure turbulent kinetic energy dissipation rates ( $\varepsilon$ ) over the upper ocean. Microstructure data were processed using the routines provided by Rockland Scientific Inc. (ODAS 4.4). It is worth noting that, on average, the mixed layer depth (MLD) was around 20 m. The MLD is defined to be the shallowest depth where the density difference is 0.03 kg m<sup>-3</sup> from the surface layer (de Boyer Montégut et al., 2004), so the processes studied here are mostly 2x to 10x below the mixed layer.

#### 2.2. Methods

The 2D form of quasi-geostrophic (QG) omega equation (Hoskins et al., 1978) is employed to compute vertical velocity *w*:

$$N^2 w_{rr} + f^2 w_{rz} = -2(u_r b_r)_r. (1)$$

Here, N is the buoyancy frequency, f is the Coriolis frequency, subscripts f and f signifies the derivatives in horizontal and vertical directions respectively, and the symbol  $\nabla_h$  signifies the horizontal gradient.  $u_r$  represents the strain field with f being the geostrophic flows calculated from SLA, and f denotes the buoyancy gradient (f be f buoyancy is negligible), f is the SLA contours). Here, f is the cross-front direction (the along-front gradient of buoyancy is negligible), f is the gravity, f is the density, and f and f buoyancy is negligible), f is the boundaries and the variables in the observational gap below the surface are also initially set to be zero (See Supporting Information S1 for the discussions on the assumptions and boundaries for the Omega equation). Note that the diagnosed f may be inaccurate near the boundaries.

The VHT is defined as:

$$VHT = \rho C_p w' T', \tag{2}$$

where  $C_p = 4007 \text{ J kg}^{-1} \text{ K}^{-1}$  is the specific heat capacity of sea water, and w' and T' are the anomalies of vertical velocity and temperature after removing the sectional mean, respectively. To compare the effects of mesoscale and submesoscale processes on VHT, we classify the motions smaller than 30 km as submesoscale-dominated processes ( $w_s'$  and  $T_s'$ ). Applying a 30-km moving averge on w' and T' and then substracting the average from the original values to obtain submesoscale-dominated VHT<sub>s</sub> as follows,

$$VHT_s = \rho C_n w_s' T_s'. \tag{3}$$

Thus, the mesoscale-dominated component can be calculated by

$$VHT_{m} = VHT - VHT_{c}.$$
 (4)

Turbulent heat flux, F<sub>H</sub>, can be estimated using the following expression:

$$F_{\rm H} = -\rho C_p K_\rho \frac{\partial T}{\partial z}.$$
 (5)

Here,  $K_{\rho}$  is the density diffusivity estimated using the Osborn (1980) equation,  $K_{\rho} = \Gamma \varepsilon / N^2$ , where  $\Gamma$  is the mixing coefficient set as 0.2 (Gregg et al., 2018). Positive (negative) values denote upward (downword) heat flux.

#### 3. Results

#### 3.1. Vertical Velocity, Temperature Anomaly, and VHT

Disregarding the influence of large-scale vertical velocity and taking the diagnosed vertical velocity to be dominated by the anomaly, we have w' = w. For the eddy case, the representative section S3 was selected since it

CAO ET AL. 3 of 9

19448007, 2024, 12, Downloaded from https://agupubs.onlinelibrary.wiley.com/doi/10.1029/2024GL110190, Wiley Online Library on [17/06/2024]. See the Terms and Conditions (https://online

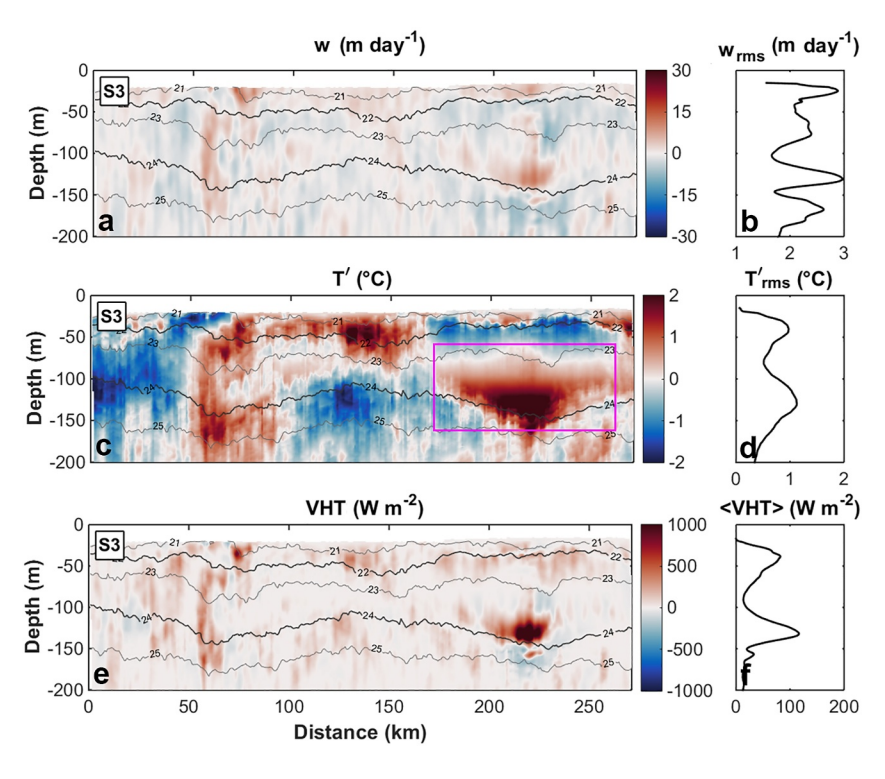


Figure 2. Vertical section of (a) diagnosed vertical velocity w derived from the quasi-geostrophic Omega Equation 1, (c) temperature anomaly (T') from observations, and (e) vertical heat transport (VHT) along the cross-eddy section (marked as S3 in Figure 1b). The black solid lines indicate the isopycnals. The root-mean-square values of (b) w and (d) T' as a function of depth. (f) Averaged VHT, with the bracket indicating the sectional average.

cleanly intersected the target eddy. As shown in Figure 2a, the diagnosed vertical velocity over the upper 200 m exhibits a limited range between  $\pm 10$  m day<sup>-1</sup>. This behavior is likely due to the relatively weak strain rate within the mesoscale eddy, despite the significant buoyancy gradients (Figure S5a in Supporting Information S1). The temperature along this section displays a prominent anomaly within the range of  $\pm 2^{\circ}$ C (Figure 2c), with both mesoscale and submesoscale signatures. The root-mean-square (RMS) value of T decreases rapidly below 150 m, suggesting that the dominant dynamics primarily operate within the upper 200 m. Notably, a distinct subsurface eddy core with a length scale of approximately 100 km, highlighted by a magenta rectangle, was observed between isopycnals of 22 and 24 kg m<sup>-3</sup>. At the base of the eddy core, a prominent peak of upward VHT reaches 1000 W m<sup>-2</sup> (Figure 2e), as a consequence of enhanced w' and T' with the same sign, in this case warm water moving upward. The large w' could be ascribed to the weak stratification (small N) in the core (Figure S5b in Supporting Information S1). Thus, although the VHT is well below the surface mixed layer it is nearby a lowstratification anomaly. Given the observed substantial T' there (Figure 2c), the VHT becomes extremely large at the base of the eddy core. We suppose that this remarkable VHT would persist through out the life cycle of the eddy core. Across the entire observational transect, the positive VHT values substantially outweigh the negative values, culminating in a net upward VHT over the upper 200 m (Figure 2f) and indicating a release of potential energy (Fox-Kemper et al., 2008), which is consistent with both frontogenesis and baroclinic instability (McWilliams, 2016). The consistent upward VHT is unlikely dominated by errors from internal wave or instrument noise contamination.

Figure 3 presents the characteristics of vertical velocity, temperature anomaly, and VHT across the fronts F1-F7. Unlike Section S3, F1-F7 consists of seven cross-front sections created as the vessel traversed the fronts, as shown in Figure 1. Remarkably, at these fronts, the vertical velocity displays much larger magnitudes compared to those within the eddy (Figure 3b in comparison to Figure 2b). Along each section, we observed an alternating pattern of positive and negative w, which resembles a characteristic of frontogenesis known as ageostrophic motions at the fronts (Esposito et al., 2023; Hoskins et al., 1978). Although the  $T'_{rms}$  at the fronts tends to be smaller than that of S3 (Figure 3d compared to Figure 2d), a clear frontal pattern along with smaller-scale features is present in each

CAO ET AL. 4 of 9

19448007, 2024, 12, Downloaded from https://agupubs.onlinelibrary.wiley.com/doi/10.1029/2024GL110190, Wiley Online Library on [17/06/2024]. See the Terms and Conditional Cond

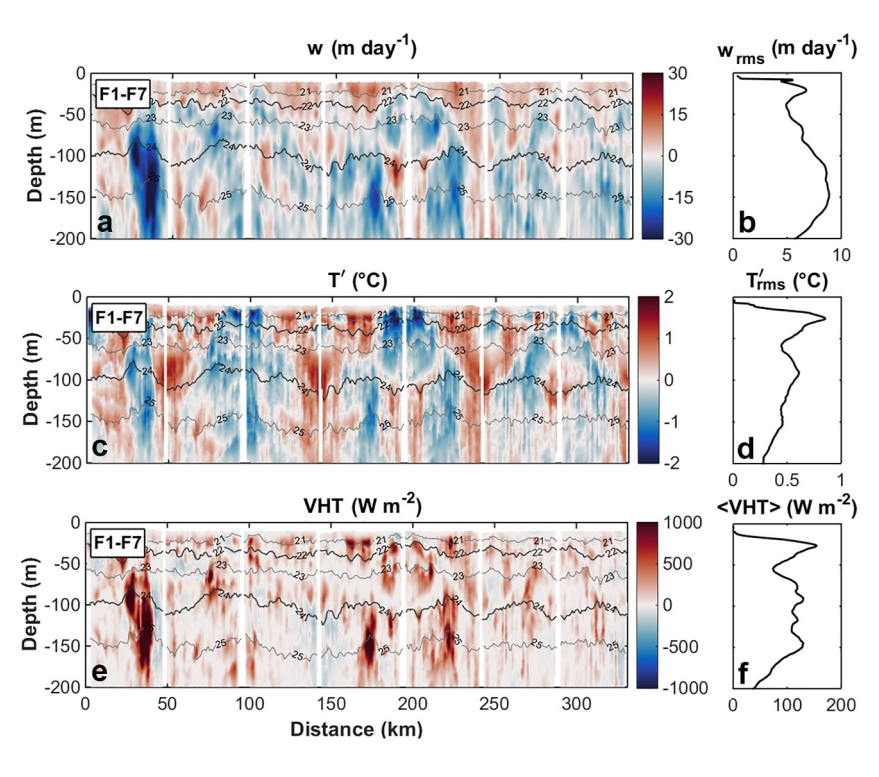


Figure 3. Same as Figure 2 but for cross-front sections F1-F7.

sub-section (Figure 3c), similar to the buoyancy gradient plot (Figure S5c in Supporting Information S1). This implies the possible frontogenesis across the scales, inducing ageostrophic motions with enhanced vertical velocity. The frontal section displays robust upward VHT, with local amplitudes strikingly reaching up to  $1000 \, \mathrm{W \, m^{-2}}$  (Figure 3e). Consequently, the averaged VHT is directed upward and reaches a magnitude exceeding  $100 \, \mathrm{W \, m^{-2}}$  before gradually decreasing below 150 m. The satellite data suggest that persistence of these fronts throughout the observation period and potentially even longer—that is, the substantial upward VHT at these fronts are not transient processes but rather as enduring phenomena, as long as the mesoscale strain persists. The upward VHT can also be explained by the correlation between vertical velocity and temperature anomalies, especially at the fronts when closer to the surface but still well below the mixed layer (Figure S6 in Supporting Information S1).

#### 3.2. Turbulent Mixing and Associated Heat Flux

Dissipative processes at finer scales would also contribute to the VHT, which was investigated using the observed turbulent kinetic energy dissipation rates ( $\epsilon$ ). By assuming the same diffusivity for heat and density in fully developed turbulence, we can estimate turbulent heat flux by Equation 5. Here the VMP casts were categorized into two groups: those conducted within the eddy and those performed at the fronts, so as to compare the turbulent mixing and the associated heat flux in these two regions. As illustrated in Figure 4,  $\epsilon$  reach magnitudes of up to  $1 \times 10^{-6}$  W kg<sup>-1</sup> at the near surface layer and quickly decrease to  $1 \times 10^{-9}$  to  $1 \times 10^{-8}$  W kg<sup>-1</sup> below 25 m (the base of the mixed layer). On average, the  $\epsilon$  within the eddy tend to be approximately 3–8 times greater than those at the fronts over the upper 50 m (Figure 4c). Within deeper layers the two regions exhibit similar  $\epsilon$  levels. Notably, the subsurface fronts do not markedly elevate local dissipation rates within the stratified layer, differing from the pattern observed within the mixed layer (Dong et al., 2022; Yang et al., 2017). The similar trends are discerned in the vertical distribution of diffusivity and turbulent heat flux (Figures 4f and 4i). In summary, turbulent mixing in the ocean interior accounts for a limited downward heat flux ranging from 0.5 to 10 W m<sup>-2</sup> (Figure 4i), which is insufficient to offset the locally strong upward beat flux associated with mesoscale and submesoscale processes (Figure 5). This implies that the strong upward VHT at the fronts can effectively heat the subsurface, potentially leading to increased stratification (Figure S5d in Supporting Information S1). This

CAO ET AL. 5 of 9

1944/8007, 2024, 12, Downloaded from https://agupubs.onlineibitary.wile.co.or/doi/10.1029/2024GL110190, Wiley Online Library on [17/06/2024]. See the Terms and Conditions (https://onlineibitary.wiley.com/terms-and-conditions) on Wiley Online Library for rules of use; OA articles are governed by the applicable Creative

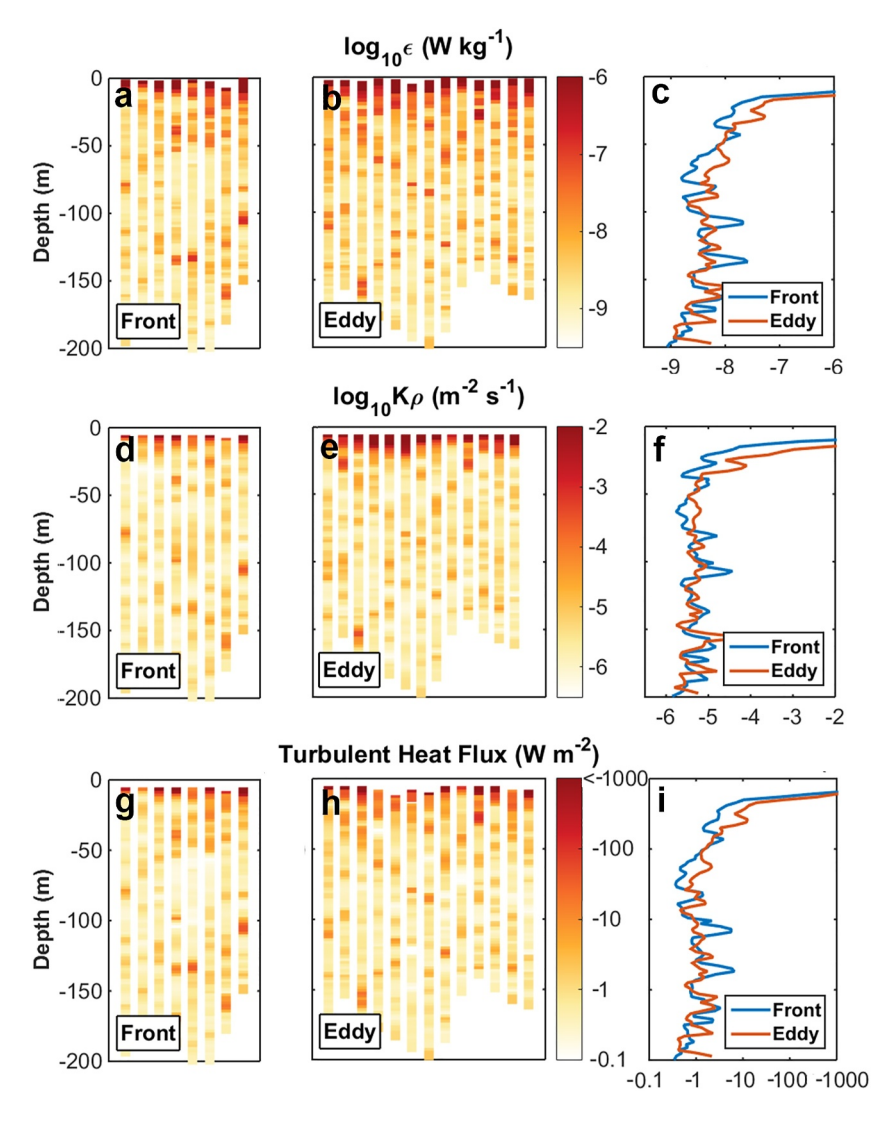


**Figure 4.** Observed turbulent kinetic energy dissipation rates  $(\varepsilon)$  from the casts (a) at the fronts and (b) within the eddy. The diffusivity  $(K_{\rho})$  estimated (d) at the fronts and (e) within the eddy. The estimated turbulent heat flux (g) at the fronts and (h) within the eddy. (c, f, and i) Present a comparision of averaged  $\varepsilon$ ,  $K_{\rho}$ , and turbulent heat flux in these two regions. The turbulent heat flux is directed downward with negative values.

enhanced stratification may act as a feedback mechanism to restrain vertical mixing, as evidenced by the weaker  $\varepsilon$  at the front in the observations.

#### 3.3. Mesoscale VS Submesoscale VHT

To compare the relative contributions of mesoscale and submesoscale processes on VHT, we utilized spectral analysis to estimate the spectral VHT by calculating the cospectrum of vertical velocity and temperature anomaliy (Su et al., 2020). This approach, as demonstrated in previous studies (e.g., Cao et al., 2021, 2023; Torres et al., 2018), can effectively identify dominant length scales of motions and their respective contributions. Given that temperature serves as a tracer and vertical velocity acts as an independent variable in horizontal scales, their cospectrum represents the VHT as a function of scale  $(\rho C_p \widehat{w'T'}^*)$ , where \*indicates the complex conjugate). Concerning the limited length of the sections, we applied a periodic boundary condition during spectral analysis to mitigate the Gibbs effects. Figures 5a and 5c illustrate the spectral variances as a function of length scales (wavenumber) in the upper 200 m, which are mostly positive. At the fronts, submesoscale contributions (<30 km) to VHT are remarkable at all depths (Figure 5a), resulting in a strong net upward VHT exceeding 100 W m<sup>-2</sup>

CAO ET AL. 6 of 9

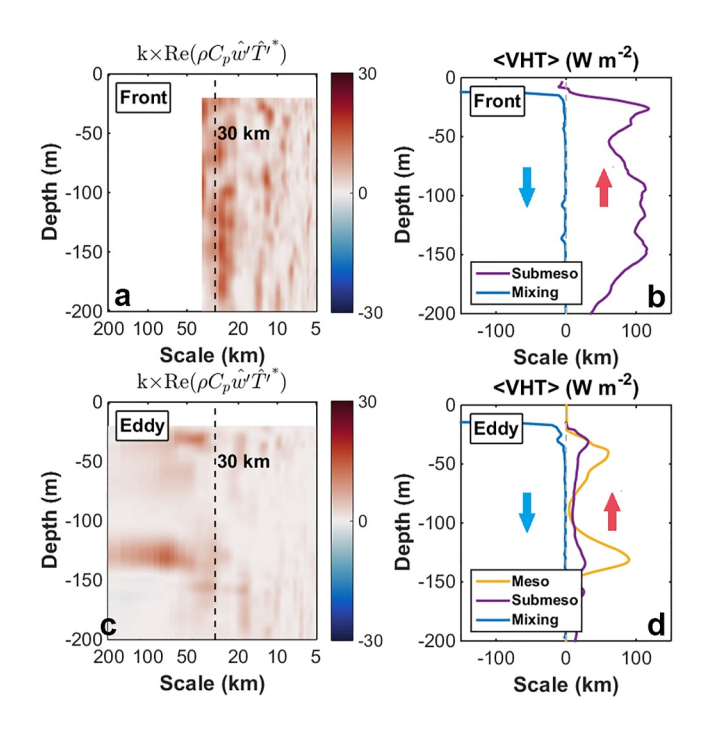


**Figure 5.** (a) Upper-ocean spectral variances of the cospectrum of vertical velocity and temperature anomaly for the (a) frontal and (c) eddy regions. The dashed line indicate the length scale of 30 km. A summay of averaged vertical heat transport (VHT) by mesoscale, submesoscale, and turbulent-scale processes in the (b) frontal and (d) eddy regions. The red (blue) arrows indicate upward (downward) VHT.

between the depth range of 25–150 m (Figure 5b). Note that the mesoscale effects on VHT at the fronts may be somewhat deceptive, as section F1-F7 comprises multiple segments (each cross-front section being approximately 50 km). By contrast, the cospectrum for the eddy case exhibits much smaller variances, especially in the submesoscale range (Figure 5c). As shown in Figure 5d, the upward VHT within the eddy primarily results from mesoscale processes (a vertically averaged value of 22 W m<sup>-2</sup>) rather than from submesoscale processes (a vertically averaged value of 16 W m<sup>-2</sup>). The conspicuous peak near 130 m corresponds to the effects of the subsurface eddy mentioned before.

In both the eddy and frontal regions, mesoscale and submesoscale processes caused a significant imbalance in local VHT, while pronounced downward VHT by dissipative processes only were observed within the upper 25 m. In particular, the averaged upward VHT induced by the deep-reaching fronts reaches a considerable magnitude exceeding 100 W m<sup>-2</sup> well below the mixed layer (25-150 m). Although smaller than the estimated wintertime VHT associated with mixed-layer submesoscale dynamics (Fox-Kemper & Ferrari, 2008; Su et al., 2018), it is an order of magnitude larger than the contribution from mesoscale eddies alone, which are traditionally considered as the main driver of upward VHT within the stratified interior (Wolfe et al., 2008). This value is also comparable to, or even larger than, the climatological net air-sea heat fluxes in this region (Large & Yeager, 2009). Although the observations only provide a snapshot of the enhanced VHT, as mentioned above, both mesoscale eddies and the fronts between eddies would persist over extended durations (weeks to months), as indicated by sea level anomalies of satellite altimetry. These results highlight a potential coherent pathway that links the ocean interior and the atmosphere, and this may be an ubiquitous phenomenon in eddy-riched oceans.

#### 4. Conclusions and Discussions

This study employed high-resolution observations targeting mesoscale eddies and fronts between eddies to investigate the VHT in the subsurface layer. This direct observational evidence for vertical transport pathways between the ocean surface and interior results from advancements in fast-sampling technology of TRIAXUS, capable of capturing submesoscale signatures in the eddy-active South China Sea. Despite observational limitations, approximations, and assumptions (particularly in estimating vertical velocity), our observation-based results allow for a comparison of VHT associated with meso-, submeso-, and turbulent processes, respectively. Notably, this study highlights the significant role of the deep-reaching fronts between eddies in driving consistent upward VHT, which reaches up to 100 W m<sup>-2</sup>. The VHT here is through frontogenesis processes, which tend to transport heat vertically, but along tilted isopycnals rather than through diapycnal mixing. Also, this high upward VHT can not be compensated by local mixing and plays a pivotal role in heating the subsurface. These findings challenge the conventional belief that enhanced stratification eliminates surface-to-depth exchange and decouples surface and subsurface waters (Rosso et al., 2014; Sallée et al., 2021), although the subsurface vertical mixing tends to be restrained due to the stratification enhancement by upward VHT.

Our results emphasize the need to consider small-scale physics not only within the ocean surface mixed layer but also below it, when assessing oceanic heat uptake. In the moderate strain field, the strain-induced lateral buoyancy gradients and frontal dynamics in the subsurface layer emerge as the primary mechanism for upward VHT, crucially accounting for the vertical exchange between the ocean surface and interior. An assessment of the non-dimensional Ertel potential vorticity ( $q = 1 + Ro - Ri^{-1}$ ) suggests that these processes are not predominately linked to small-scale instabilities (e.g., centrifugal-symmetric instabilities, which could trigger turbulent mixing; see Figure S7 in Supporting Information S1). Note that, currently, there has not been an adequate parameterization for these upward VHT in the subsurface. Inaccurate representation of such physics could significantly underestimate the VHT imbalance in the upper ocean (Siegelman et al., 2020).

CAO ET AL. 7 of 9

Acknowledgments

Key R&D Program of China

This study was supported by the National

(2023YFC3008003) and the National

Natural Science Foundation of China

42149907, 42349907, and 42349584).

and all technical and scientific staff

during the cruise (NORC2022-302).

Special thanks are extended to Ruixi

data. Prof. Xiangzhou Song is

insightful discussions.

BFK was supported by NSF 2149041. The

authors are grateful to the captain and crew

involved in conducting the measurements

Zheng and Xin Meng for their dedicated

efforts in collecting and processing the raw

acknowledged for valuable comments and

(42225602, 42176004, 92258301,

The most significant uncertainties arise from the possible contamination by the internal wave motions during the estimates, although no clear wave-induced signal is observed in the VHT plots, and on average they did not contribute to net VHT (Siegelman, 2020; Wang et al., 2022). If VHT is predominantly influenced by internal wave motions, little distinction would be seen between the eddy and front cases. The vertical transport of passive and biological tracers may be associated with submesoscale along-isopycnal stirring through both frontogenesis and small-scale instabilities (Cao et al., 2024). Further observations and insightful analyses, alongside numerical modeling, are imperative for a comprehensive understanding of the underlying dynamics. The enhanced vertical transport associated with these submeso- and smaller-scale processes holds significant implications for improving our understanding of climate and biogeochemical systems.

#### **Data Availability Statement**

The sea level anomaly and geostrophic currents are derived from satellite altimeter data (AVISO) or from the Copernicus Marine Environment Monitoring Service (Global Ocean Gridded L4 Sea Surface Heights And Derived Variables Reprocessed, 1993 Ongoing, 2023). The data used for analysis in this study are available in Cao (2023).

#### References

- Boccaletti, G., Ferrari, R., & Fox-Kemper, B. (2007). Mixed layer instabilities and restratification. *Journal of Physical Oceanography*, 37(9), 2228–2250. https://doi.org/10.1175/JPO3101.1
- Bodner, A. S., Fox-Kemper, B., Johnson, L., Van Roekel, L. P., McWilliams, J. C., Sullivan, P. P., et al. (2023). Modifying the mixed layer eddy parameterization to include frontogenesis arrest by boundary layer turbulence. *Journal of Physical Oceanography*, 53(1), 323–339. https://doi.org/10.1175/JPO-D-21-0297.1
- Bryan, K. (1996). The role of mesoscale eddies in the poleward transport of heat by the oceans: A review. *Physica D: Nonlinear Phenomena*, 98(2–4), 249–257. https://doi.org/10.1016/0167-2789(96)00119-4
- Callies, J., Ferrari, R., Klymak, J. M., & Gula, J. (2015). Seasonality in submesoscale turbulence. Nature Communication, 6(1), 6862. https://doi. org/10.1038/ncomms/862
- Cao, H. (2023). SCS\_CRUISE DATA [Dataset]. Zenodo. https://doi.org/10.5281/zenodo.10339160
- Cao, H., Fox-Kemper, B., & Jing, Z. (2021). Submesoscale eddies in the upper ocean of the Kuroshio extension from high-resolution simulation: Energy budget. *Journal of Physical Oceanography*, 51(7), 2181–2201. https://doi.org/10.1175/JPO-D-20-0267.1
- Cao, H., Fox-Kemper, B., Jing, Z., Song, X., & Liu, Y. (2023). Towards the upper-ocean unbalanced submesoscale motions in the oleander observations. *Journal of Physical Oceanography*, 53(4), 1123–1138. https://doi.org/10.1175/JPO-D-22-0134.1
- Cao, H., Freilich, M., Song, X., Jing, Z., Fox-Kemper, B., Qiu, B., et al. (2024). Isopycnal submesoscale stirring crucially sustaining subsurface chlorophyll maximum in ocean cyclonic eddies. *Geophysical Research Letters*, 51(4), e2023GL105793. https://doi.org/10.1029/ 2023GL105793
- Cao, H., & Jing, Z. (2022). Submesoscale ageostrophic motions within and below the mixed layer of the northwestern Pacific Ocean. *Journal of Geophysical Research: Oceans*, 127(2), e2021JC017812, https://doi.org/10.1029/2021JC017812
- Cutolo, E., Pascual, A., Ruiz, S., Shaun Johnston, T. M., Freilich, M., Mahadevan, A., et al. (2022). Diagnosing frontal dynamics from observations using a variational approach. *Journal of Geophysical Research: Oceans*, 127(11), e2021JC018336. https://doi.org/10.1029/2021JC018336
- de Boyer Montégut, C., Madec, G., Fischer, A., Lazar, A., & Iudicone, D. (2004). Mixed layer depth over the global ocean: An examination of profile data and a profile-based climatology. *Journal of Geophysical Research*, 109(C12), C12003. https://doi.org/10.1029/2004JC002378
- Dong, C., McWilliams, J. C., Liu, Y., & Chen, D. (2014). Global heat and salt transports by eddy movement. *Nature Communications*, 5(1), 3294. https://doi.org/10.1038/ncomms4294
- Dong, J., Fox-Kemper, B., Jing, Z., Yang, Q., Tian, J., & Dong, C. (2022). Turbulent dissipation in the surface mixed layer of an anticyclonic mesoscale eddy in the South China Sea. *Geophysical Research Letters*, 49(16), e2022GL100016. https://doi.org/10.1029/2022GL10001
- Dong, J., Fox-Kemper, B., Zhang, H., & Dong, C. (2020). The scale of submesoscale baroclinic instability globally. *Journal of Physical Oceanography*, 50(9), 2649–2667. https://doi.org/10.1175/JPO-D-20-0043.1
- Esposito, G., Donnet, S., Berta, M., Shcherbina, A. Y., Freilich, M., Centurioni, L., et al. (2023). Inertial oscillations and frontal processes in an Alboran Sea jet: Effects on divergence and vertical transport. *Journal of Geophysical Research: Oceans*, 128(3), e2022JC019004. https://doi.org/10.1029/2022JC01900
- Ferrari, R. (2011). A frontal challenge for climate models. Science, 332(6027), 316-317. https://doi.org/10.1126/science.1203632
- Ferrari, R., & Wunsch, C. (2009). Ocean circulation kinetic energy: Reservoirs, sources, and sinks. *Annual Review of Fluid Mechanics*, 41(1), 253–282. https://doi.org/10.1146/annurev.fluid.40.111406.102139
- Fox-Kemper, B., Danabasoglu, G., Ferrari, R., Griffies, S., Hallberg, R., Holland, M., et al. (2011). Parameterization of mixed layer eddies. III: Implementation and impact in global ocean climate simulations. *Ocean Modelling*, 39(1–2), 61–78. https://doi.org/10.1016/j.ocemod.2010. 09.002
- Fox-Kemper, B., & Ferrari, R. (2008). Parameterization of mixed layer eddies. Part II: Prognosis and impact. *Journal of Physical Oceanography*, 38(6), 1166–1179. https://doi.org/10.1175/2007JPO3788.1
- Fox-Kemper, B., Ferrari, R., & Hallberg, R. (2008). Parameterization of mixed layer eddies. Part I: Theory and diagnosis. *Journal of Physical Oceanography*, 38(6), 1145–1165. https://doi.org/10.1175/2007JPO3792.1
- Global Ocean gridded L4 Sea surface heights and derived variables reprocessed 1993 ongoing. (2023). Global Ocean gridded L4 Sea surface heights and derived variables reprocessed 1993 ongoing [dataset]. E.U. Copernicus Marine Service Information (CMEMS). https://doi.org/10.48670/moi-00148
- Gregg, M. C., D'Asaro, E. A., Riley, J. J., & Kunze, E. (2018). Mixing efficiency in the ocean. Annual Review of Marine Science, 10(1), 443–473. https://doi.org/10.1146/annurev-marine-121916-063643

CAO ET AL. 8 of 9

- Griffies, S. M., Winton, M., Anderson, W. G., Benson, R., Delworth, T. L., Dufour, C. O., et al. (2015). Impacts on ocean heat from transient mesoscale eddies in a hierarchy of climate models. *Journal of Climate*, 28(3), 952–977. https://doi.org/10.1175/JCLI-D-14-00353.1
- Hoskins, B. J., Draghici, I., & Davies, H. C. (1978). A new look at the ω-equation. Quarterly Journal of the Royal Meteorological Society, 104(439), 31–38. https://doi.org/10.1002/qj.49710443903
- Jayne, S. R., & Marotzke, J. (2002). The oceanic eddy heat transport. *Journal of Physical Oceanography*, 32(12), 3328–3345. https://doi.org/10.1175/1520-0485(2002)032<3328:TOEHT>2.0.CO;2
- Jing, Z., Wang, S., Wu, L., Chang, P., Zhang, Q., Sun, B., et al. (2020). Maintenance of mid-latitude oceanic fronts by mesoscale eddies. *Science Advances*, 6(31), eaba7880. https://doi.org/10.1126/sciadv.aba7880
- Klein, P., Hua, B. L., Lapeyre, G., Capet, X., Le Gentil, S., & Sasaki, H. (2008). Upper ocean turbulence from high-resolution 3D simulations. Journal of Physical Oceanography, 38(8), 1748–1763. https://doi.org/10.1175/2007JPO3773.1
- Klein, P., & Lapeyre, G. (2009). The oceanic vertical pump induced by mesoscale and submesoscale turbulence. Annual Review of Marine Science, 1, 351–375. https://doi.org/10.1146/annurev.marine.010908.163704
- Large, W., & Yeager, S. G. (2009). The global climatology of an interannually varying air–sea flux data set. Climate Dynamics, 33(2–3), 341–364. https://doi.org/10.1007/s00382-008-0441-3
- Li, D., Chang, P., Ramachandran, S., Jing, Z., Zhang, Q., Kurian, J., et al. (2021). Contribution of the two types of Ekman pumping induced eddy heat flux to the total vertical eddy heat flux. Geophysical Research Letters, 48(9), e2021GL092982. https://doi.org/10.1029/2021GL092982
- McWilliams, J. C. (2016). Submesoscale currents in the ocean. *Proceedings of the Royal Society A: Mathematical, Physical and Engineering Sciences*, 472(2189), 20160117. https://doi.org/10.1098/rspa.2016.0117
- Osborn, T. R. (1980). Estimates of the local rate of vertical diffusion from dissipation measurements. *Journal of Physical Oceanography*, 10(1), 83–89. https://doi.org/10.1175/1520-0485(1980)010<0083:EOTLRO>2.0.CO;2
- Qu, Y., Wang, S., Jing, Z., Wang, H., & Wu, L. (2022). Spatial structure of vertical motions and associated heat flux induced by mesoscale eddies in the upper Kuroshio-Oyashio extension. *Journal of Geophysical Research: Oceans*, 127(10), e2022JC018781. https://doi.org/10.1029/2022JC018781
- Ramachandran, S., Tandon, A., & Mahadevan, A. (2014). Enhancement in vertical fluxes at a front by mesoscale-submesoscale coupling. *Journal of Geophysical Research: Oceans*, 119(12), 8495–8511. https://doi.org/10.1002/2014JC010211
- Rosso, I., Hogg, A. M., Strutton, P. G., Kiss, A. E., Matear, R., Klocker, A., & van Sebille, E. (2014). Vertical transport in the ocean due to submesoscale structures: Impacts in the Kerguelen region. *Ocean Modelling*, 80, 10–23. https://doi.org/10.1016/j.ocemod.2014.05.001
- Rudnick, D. L., & Cole, S. T. (2011). On sampling the ocean using underwater gliders. *Journal of Geophysical Research*, 116(C8), C08010. https://doi.org/10.1029/2010JC006849
- Sallée, J. B., Pellichero, V., Akhoudas, C., Pauthenet, E., Vignes, L., Schmidtko, S., et al. (2021). Summertime increases in upper-ocean stratification and mixed-layer depth. *Nature*, 591(7851), 592–598. https://doi.org/10.1038/s41586-021-03303-x
- Siegelman, L. (2020). Energetic submesoscale dynamics in the ocean interior. *Journal of Physocal Oceanography*, 50(3), 727–749. https://doi.org/10.1175/JPO-D-19-0253.1
- Siegelman, L., Klein, P., Rivière, P., Thompson, A. F., Torres, H. S., Flexas, M., & Menemenlis, D. (2020). Enhanced upward heat transport at deep submesoscale ocean fronts. *Nature Geoscience*, 13(1), 50–55. https://doi.org/10.1038/s41561-019-0489-1
- Su, Z., Torres, H., Klein, P., Thompson, A. F., Siegelman, L., Wang, J., et al. (2020). High-frequency submesoscale motions enhance the upward vertical heat transport in the global ocean. *Journal of Geophysical Research: Oceans*, 125(9), e2020JC016544. https://doi.org/10.1029/2020JC016544
- Su, Z., Wang, J., Klein, P., Thompson, A. F., & Menemenlis, D. (2018). Ocean submesoscales as a key component of the global heat budget. Nature Communications, 9(1), 775. https://doi.org/10.1038/s41467-018-02983-w
- Torres, H. S., Klein, P., Menemenlis, D., Qiu, B., Su, Z., Wang, J., et al. (2018). Partitioning ocean motions into balanced motions and internal gravity waves: A modeling study in anticipation of future space missions. *Journal of Geophysical Research: Oceans*, 123(11), 8084–8105. https://doi.org/10.1029/2018JC014438
- Wang, Q., Dong, C., Dong, J., Zhang, H., & Yang, J. (2022). Submesoscale processes-induced vertical heat transport modulated by oceanic mesoscale eddies. Deep Sea Research Part II: Topical Studies in Oceanography, 202, 105138. https://doi.org/10.1016/j.dsr2.2022.105138
- Wolfe, C. L., Cessi, P., McClean, J. L., & Maltrud, M. E. (2008). Vertical heat transport in eddying ocean models. Geophysical Research Letters, 35(23), https://doi.org/10.1029/2008GL036138
- Wunsch, C., & Ferrari, R. (2004). Vertical mixing, energy, and the general circulation of the oceans. *Annual Review of Fluid Mechanics*, 36(1), 281–314. https://doi.org/10.1146/annurev.fluid.36.050802.122121
- Yang, P., Jing, Z., Sun, B., Wu, L., Qiu, B., Chang, P., & Ramachandran, S. (2021). On the upper-ocean vertical eddy heat transport in the Kuroshio extension. Part I: Variability and dynamics. *Journal of Physical Oceanography*, 51(1), 229–246. https://doi.org/10.1175/JPO-D-20-0068.1
- Yang, Q., Zhao, W., Liang, X., Dong, J., & Tian, J. (2017). Elevated mixing in the periphery of mesoscale eddies in the South China Sea. *Journal of Physical Oceanography*, 47(4), 895–907. https://doi.org/10.1175/JPO-D-16-0256.1
- Yu, X., Naveira Garabato, A. C., Martin, A. P., Buckingham, C. E., Brannigan, L., & Su, Z. (2019). An annual cycle of submesoscale vertical flow and restratification in the upper ocean. *Journal of Physical Oceanography*, 49(6), 1439–1461. https://doi.org/10.1175/JPO-D-18-0253.1

#### **References From the Supporting Information**

- BIPM. (2008). Evaluation of measurement data: Guide to the expression of uncertainty in measurement (JCGM 100:2008, GUM 1995 with minor corrections). BIPM.
- Mahadevan, A., & Tandon, A. (2006). An analysis of mechanisms for submesoscale vertical motion at ocean fronts. *Ocean Modelling*, 14(3–4), 241–256. https://doi.org/10.1016/j.ocemod.2006.05.006
- Rudnick, D. L. (1996). Intensive surveys of the Azores front: 2. Inferring the geostrophic and vertical velocity fields. *Journal of Geophysical Research*, 101(C7), 16291–16303. https://doi.org/10.1029/96JC01144
- Rudnick, D. L., Zarokanellos, N. D., & Tintoré, J. (2022). A four-dimensional survey of the Almeria–Oran front by underwater gliders: Tracers and circulation. *Journal of Physical Oceanography*, 52(2), 225–242. https://doi.org/10.1175/JPO-D-21-0181.1
- Troupin, C., Beltran, J. P., Heslop, E., Torner, M., Garau, B., Allen, J., et al. (2015). A toolbox for glider data processing and management. Methods in Oceanography, 13–14, 13–23. https://doi.org/10.1016/j.mio.2016.01.001

CAO ET AL. 9 of 9